

Voltage/Pitch Control for Maximization and Regulation of Active/Reactive Powers in Wind Turbines with Uncertainties

Yi Guo, S. Hossein Hosseini, John N. Jiang, Choon Yik Tang, and Rama G. Ramakumar

Abstract—This paper addresses the problem of controlling a variable-speed wind turbine with a Doubly Fed Induction Generator (DFIG), modeled as an electromechanically-coupled nonlinear system with rotor voltages and blade pitch angle as its inputs, active and reactive powers as its outputs, and most of the aerodynamic and mechanical parameters as its uncertainties. Using a blend of linear and nonlinear control strategies (including feedback linearization, pole placement, uncertainty estimation, and gradient-based potential function minimization) as well as time-scale separation in the dynamics, we develop a controller that is capable of maximizing the active power in the *Maximum Power Tracking* (MPT) mode, regulating the active power in the *Power Regulation* (PR) mode, seamlessly switching between the two modes, and simultaneously adjusting the reactive power to achieve a desired power factor. The controller consists of four cascaded components, uses realistic feedback signals, and operates without knowledge of the C_p -surface, air density, friction coefficient, and wind speed. Finally, we show the effectiveness of the controller via simulation with a realistic wind profile.

Index Terms—Wind energy, wind turbine, active power, reactive power, maximum power tracking, power regulation, nonlinear control.

I. INTRODUCTION

A high-performance controller is essential to the success of integrating large-scale wind energy into future power systems. Extensive investigations and recent lessons learned have confirmed that the variable and intermittent nature of wind indeed poses serious threats to both the reliability of power systems and the economic viability of wind energy [1]. To minimize these threats, a wind turbine controller should not only maximize the amount of active power captured in a so-called *Maximum Power Tracking* (MPT) mode in normal situations, it should also allow the power captured be continuously regulated at a desired level in a so-called *Power Regulation* (PR) mode (other than clipping the power based on received instructions) when there is a system contingency. In addition, the controller should enable seamless switching

Yi Guo, S. Hossein Hosseini, John N. Jiang, and Choon Yik Tang are with the School of Electrical and Computer Engineering, University of Oklahoma, Norman, OK 73019 USA (e-mail: {yi.guo,s.h.hosseini,jnjiang,cytang}@ou.edu).

Rama G. Ramakumar is with the School of Electrical and Computer Engineering, Oklahoma State University, Stillwater, OK 74078 USA (e-mail: ramakum@okstate.edu).

This work was supported by the National Science Foundation under grants ECCS-0926038 and ECCS-0955265.

This paper is a preprint of a paper submitted to IET Renewable Power Generation and is subject to Institution of Engineering and Technology Copyright. If accepted, the copy of record will be available at IET Digital Library.

between the MPT and PR modes, as well as maintain a desired power factor by also controlling the reactive power output.

One of the challenges facing the development of such a high-performance controller is the fact that the aerodynamic and mechanical parameters of a wind turbine are inherently uncertain, due to modeling and measurement errors, unknown optimal operating points, and other, possibly time-varying, ambient factors. For example, the C_p -surface of a wind turbine, which characterizes the amount of mechanical energy converted from the wind, is typically assumed to be known—or, at least, its optimal points are assumed to be known—in many existing controller designs. Unfortunately, such a surface is an empirical, statistical approximation, obtained based on up to three months of continuous experiment [2]. Thus, the C_p -surface may not be precisely known for control purposes. Other factors, such as changes in air density due to weather, variations in friction under different operating conditions, and measurement errors due to anemometer location, also contribute to the uncertainties. Indeed, a report from the National Renewable Energy Laboratory (NREL) [3], which describes the result of its long-term test on different controllers operating on real, MW-level wind turbines, shows that the impact of these uncertainties on controller performance is significant and should be accounted for in controller design.

Another major challenge facing the development of such a high-performance controller is the fact that the mechanical and electrical parts of a modern wind turbine, which uses a Doubly Fed Induction Generator (DFIG), are tightly coupled. As will be detailed below, most studies have adopted a standard approach in the analysis and control of synchronous electric machines, in which the active and reactive powers are considered decoupled. With this approach, the active and reactive powers are adjusted via control of the mechanical and electrical parts, respectively, independent of each other. However, although a DFIG has some features of a synchronous machine, it is by nature an induction machine that exhibits strong electromechanical coupling among its rotor excitation current, rotor angular velocity, and electromagnetic torque. Hence, for performance reasons, the mechanical and electrical parts of a wind turbine with a DFIG should be considered synergistically in controller design.

The current literature offers a large collection of wind turbine controllers, including [4]–[24]. However, as was alluded to above, most of the existing publications considered the mechanical and electrical parts separately (e.g., [4]–[14] considered only the former, while [15]–[23] considered only

the latter), and for a few of those (e.g., [24]) that considered both parts, its controller can only operate in the MPT mode, maximizing wind energy conversion, as opposed to both the MPT and PR modes. Moreover, although the existing work has provided valuable understanding in the control of wind turbines, only a few publications have addressed the issue of uncertainties. For example, [4]–[6] proposed adaptive frameworks for controlling the mechanical part of wind turbines, so that the power captured is maximized, despite not knowing the C_p -surface.

In our recent work [25], we developed a nonlinear controller that simultaneously enables control of the active power in both the MPT and PR modes, seamless switching between the two, and control of the reactive power so that a desirable power factor is maintained. These objectives were achieved by adjusting the rotor voltages of the electrical part and the blade pitch angle of the mechanical part, where the coupling between the two parts were taken into account in the controller design. Like most of the existing work, however, the controller in [25] assumed that the aerodynamic and mechanical parameters were known.

In this paper, we develop a controller that achieves such objectives and, at the same time, addresses the two aforementioned challenges, on uncertainties in the aerodynamic and mechanical parameters, and coupling between the mechanical and electrical parts. For the former, we show that the parametric uncertainties can be lumped into a scalar term, estimated via an uncertainty estimator in an inner loop, and circumvented in an outer, gradient-based minimization loop. For the latter, we show that the electromechanical coupling can be eliminated via feedback linearization on the electrical dynamics, following ideas from [25]. Finally, we demonstrate the effectiveness of the controller developed through simulation with a realistic wind profile from a wind farm in Oklahoma.

The outline of this paper is as follows: Section II models the wind turbine and formulates the problem. Section III describes the proposed controller. Section IV presents the simulation results. Finally, Section V concludes the paper. The proof of the main theorem is included in the Appendix.

II. MODELING AND PROBLEM FORMULATION

Consider a variable-speed wind turbine with a Doubly Fed Induction Generator (DFIG). The wind turbine consists of an electrical part and a mechanical part, the dynamics of which may be modeled as follows:

The dynamics of the electrical part in the dq frame are described by a fourth-order state space model [26], [27]

$$\begin{bmatrix} \dot{\varphi}_{ds} \\ \dot{\varphi}_{qs} \\ \dot{\varphi}_{dr} \\ \dot{\varphi}_{qr} \end{bmatrix} = \underbrace{\begin{bmatrix} -\frac{R_s}{\sigma L_s} & \omega_s & \frac{R_s L_m}{\sigma L_s L_r} & 0 \\ -\omega_s & -\frac{R_s}{\sigma L_s} & 0 & \frac{R_s L_m}{\sigma L_s L_r} \\ \frac{R_r L_m}{\sigma L_s L_r} & 0 & -\frac{R_r}{\sigma L_r} & \omega_s \\ 0 & \frac{R_r L_m}{\sigma L_s L_r} & -\omega_s & -\frac{R_r}{\sigma L_r} \end{bmatrix}}_A \begin{bmatrix} \varphi_{ds} \\ \varphi_{qs} \\ \varphi_{dr} \\ \varphi_{qr} \end{bmatrix}$$

$$+ \underbrace{\begin{bmatrix} 0 & 0 \\ 0 & 0 \\ 1 & 0 \\ 0 & 1 \end{bmatrix}}_B \begin{bmatrix} v_{dr} \\ v_{qr} \end{bmatrix} + \begin{bmatrix} v_{ds} \\ v_{qs} \\ -\omega_r \varphi_{qr} \\ \omega_r \varphi_{dr} \end{bmatrix}, \quad (1)$$

where $\varphi_{ds}, \varphi_{qs}, \varphi_{dr}, \varphi_{qr} \in \mathbb{R}$ are state variables representing the stator and rotor fluxes, $v_{dr}, v_{qr} \in \mathbb{R}$ are control variables representing the rotor voltages, $v_{ds}, v_{qs} \in \mathbb{R}$ are the constant stator voltages (that are not simultaneously zero), $\omega_s > 0$ is the constant angular velocity of the synchronously rotating reference frame, $\omega_r > 0$ is the rotor angular velocity, R_s, R_r are the stator and rotor resistances, L_s, L_r, L_m are the stator, rotor, and mutual inductances satisfying $L_s > L_m$ and $L_r > L_m$, $\sigma = 1 - \frac{L_m^2}{L_s L_r}$ is the leakage coefficient, and A, B are constant matrices. In addition, the fluxes can be written as [27]

$$\underbrace{\begin{bmatrix} \varphi_{ds} \\ \varphi_{qs} \\ \varphi_{dr} \\ \varphi_{qr} \end{bmatrix}}_\varphi = \begin{bmatrix} L_s & 0 & L_m & 0 \\ 0 & L_s & 0 & L_m \\ L_m & 0 & L_r & 0 \\ 0 & L_m & 0 & L_r \end{bmatrix} \underbrace{\begin{bmatrix} i_{ds} \\ i_{qs} \\ i_{dr} \\ i_{qr} \end{bmatrix}}_i, \quad (2)$$

where $i_{ds}, i_{qs}, i_{dr}, i_{qr} \in \mathbb{R}$ are the stator and rotor currents, while $\varphi = [\varphi_{ds} \varphi_{qs} \varphi_{dr} \varphi_{qr}]^T$ and $i = [i_{ds} i_{qs} i_{dr} i_{qr}]^T$ are introduced just for convenience. Furthermore, the active and reactive stator and rotor powers are given by [28]

$$P_s = -v_{ds} i_{ds} - v_{qs} i_{qs}, \quad Q_s = -v_{qs} i_{ds} + v_{ds} i_{qs}, \quad (3)$$

$$P_r = -v_{dr} i_{dr} - v_{qr} i_{qr}, \quad Q_r = -v_{qr} i_{dr} + v_{dr} i_{qr}, \quad (4)$$

and the total active and reactive powers of the turbine are

$$P = P_s + P_r, \quad Q = Q_s + Q_r, \quad (5)$$

where positive (negative) values of P and Q mean that the turbine injects power into (draws power from) the grid.

The dynamics of the mechanical part are described by a first-order state space model [26]

$$J \dot{\omega}_r = T_m - T_e - C_f \omega_r, \quad (6)$$

where the rotor angular velocity ω_r is another state variable, J is the moment of inertia, C_f is the friction coefficient, T_m is the mechanical torque, and T_e is the electromagnetic torque given by [28]

$$T_e = \varphi_{qs} i_{ds} - \varphi_{ds} i_{qs}, \quad (7)$$

where positive (negative) value of T_e means that the turbine acts as a generator (motor). The mechanical power captured by the wind turbine is [29]

$$P_m = T_m \omega_r = \frac{1}{2} \rho A C_p(\lambda, \beta) V_w^3, \quad (8)$$

where ρ is the air density, $A = \pi R^2$ is the area swept by the rotor blades of radius R , V_w is the wind speed, and $C_p(\lambda, \beta)$, commonly referred to as the C_p -surface, is the performance coefficient of the wind turbine, whose value is a function of the tip speed ratio $\lambda \in (0, \infty)$, defined as

$$\lambda = \frac{\omega_r R}{V_w}, \quad (9)$$

and the blade pitch angle $\beta \in [\beta_{\min}, \beta_{\max}]$, which is another control variable.

In order for results of this paper to be applicable to a broad class of wind turbines, no specific expression of $C_p(\lambda, \beta)$ will be assumed. Instead, $C_p(\lambda, \beta)$ will only be assumed to satisfy the following mild conditions for the purpose of analysis:

- (A1) Function $C_p(\lambda, \beta)$ is continuously differentiable in both λ and β over $\lambda \in (0, \infty)$ and $\beta \in [\beta_{\min}, \beta_{\max}]$.
- (A2) There exists $c \in (0, \infty)$ such that for all $\lambda \in (0, \infty)$ and $\beta \in [\beta_{\min}, \beta_{\max}]$, we have $C_p(\lambda, \beta) \leq c\lambda$. This condition is mild because it is equivalent to saying that the mechanical torque T_m is bounded from above, since $T_m \propto \frac{C_p(\lambda, \beta)}{\lambda}$ according to (8) and (9).
- (A3) For each fixed $\beta \in [\beta_{\min}, \beta_{\max}]$, there exists $\lambda_1 \in (0, \infty)$ such that for all $\lambda \in (0, \lambda_1)$, we have $C_p(\lambda, \beta) > 0$. This condition is also mild because turbines are designed to capture wind power over a wide range of λ , including times when λ is small.
- (A4) There exist $\underline{c} \in (-\infty, 0)$ and $\bar{c} \in (0, \infty)$ such that for all $\lambda \in (0, \infty)$ and $\beta \in [\beta_{\min}, \beta_{\max}]$, we have $\underline{c} \leq \frac{\partial}{\partial \lambda} \left(\frac{C_p(\lambda, \beta)}{\lambda} \right) \leq \bar{c}$.

As it follows from the above, the wind turbine is modeled as a fifth-order, electromechanically-coupled, nonlinear system with state equations (1) and (6), output equations (3)–(5), state variables $\varphi_{ds}, \varphi_{qs}, \varphi_{dr}, \varphi_{qr}$, and ω_r , control variables v_{dr}, v_{qr} , and β , output variables P and Q , and exogenous “disturbance” V_w . A block diagram of this system is shown on the right-hand side of Figure 1, in which the electromechanical coupling can be seen.

Given the above model, the problem addressed in this paper is: design a feedback controller, so that the active and reactive powers P and Q closely track some desired, possibly time-varying references P_d and Q_d , assumed to be provided by a wind farm operator. When P_d is larger than what the wind turbine is capable of generating, it means that the operator wants the turbine to operate in the *Maximum Power Tracking* (MPT) mode; otherwise, the *Power Regulation* (PR) mode is sought. By also providing Q_d , the operator indirectly specifies a desired power factor $\text{PF}_d = \frac{P_d}{\sqrt{P_d^2 + Q_d^2}}$, around which the actual power factor $\text{PF} = \frac{P}{\sqrt{P^2 + Q^2}}$ should be regulated. The controller may use i, ω_r, P , and Q , which are all measurable, as feedback. The fluxes φ may also be viewed as feedback, since they are bijectively related to i through (2). Moreover, the controller may use values of all the electrical parameters (i.e., $\omega_s, R_s, R_r, L_s, L_r, L_m, v_{ds}$, and v_{qs}) and turbine-geometry-dependent parameters (i.e., J, A, R, β_{\min} , and β_{\max}), since these values are typically quite accurately known. However, it may not use values of the C_p -surface, the air density ρ , and the friction coefficient C_f , since these values are inherently uncertain and can change over time. Furthermore, the controller should not rely on the wind speed V_w , since it may not be accurately measured.

III. CONTROLLER DESIGN

In this section, we address the aforementioned problem by developing a nonlinear controller consisting of four sub-controllers. Figure 1 shows the architecture of the nonlinear

controller, where each block represents a subcontroller. Note that the controller accepts P_d and Q_d as reference inputs, uses i, ω_r, P , and Q as feedback, and produces v_{dr}, v_{qr} , and β as control inputs to the wind turbine. Moreover, the different gray levels of the blocks in Figure 1 represent our intended time-scale separation in the closed-loop dynamics: the darker a block, the slower its dynamics. The subcontrollers will be described in Sections III-A–III-D. Note that Sections III-A and III-B up to the coordinate change are similar to our previous work [25], while the rest of the paper contains new, unpublished results.

A. Rotor Voltages Subcontroller

Observe that although the electrical dynamics (1) are nonlinear, they possess a nice structure: the first and second rows of (1) are affine, consisting of linear terms and the constants v_{ds} and v_{qs} , while the third and fourth are nonlinear, consisting of linear terms, the control variables v_{dr} and v_{qr} , and the nonlinearities $-\omega_r \varphi_{qr}$ and $\omega_r \varphi_{dr}$ induced by the electromechanical coupling. Since the nonlinearities enter the dynamics the same way the control variables v_{dr} and v_{qr} do, we may use *feedback linearization* [30] to cancel them and perform *pole placement* [31], i.e., let

$$v_{dr} = \omega_r \varphi_{qr} - K_1^T \varphi + u_1, \quad (10)$$

$$v_{qr} = -\omega_r \varphi_{dr} - K_2^T \varphi + u_2, \quad (11)$$

where $\omega_r \varphi_{qr}$ and $-\omega_r \varphi_{dr}$ are intended to cancel the nonlinearities, $-K_1^T \varphi$ and $-K_2^T \varphi$ with $K_1, K_2 \in \mathbb{R}^4$ are for pole placement, and u_1 and u_2 are new control variables to be designed in Section III-B.

Substituting (10) and (11) into (1), we get

$$\dot{\varphi} = (A - BK)\varphi + [v_{ds} v_{qs} u_1 u_2]^T, \quad (12)$$

where $K = [K_1 \ K_2]^T$ is the state feedback gain matrix. Since the electrical dynamics are physically allowed to be much faster than the mechanicals, we may choose K in (12) to be such that $A - BK$ is asymptotically stable with very fast eigenvalues. With K chosen as such and with relatively slow-varying u_1 and u_2 , the linear differential equation (12) may be approximated by a linear algebraic equation:

$$\varphi = -(A - BK)^{-1} [v_{ds} v_{qs} u_1 u_2]^T. \quad (13)$$

Consequently, the fifth-order state equations (1) and (6) may be approximated by the first-order state equation (6) along with algebraic relationships (10), (11), and (13). This approximation will be made in all subsequent development (but not in simulation).

Note that (2), (10), and (11) describe the *Rotor Voltages Subcontroller* block in Figure 1.

B. Electromagnetic Torque Subcontroller with Uncertainty Estimation

Having addressed the electrical dynamics, we now consider the mechanicals, where the goal is to construct a subcontroller, which makes the rotor angular velocity ω_r track a desired, slow-varying reference ω_{rd} , despite not knowing the

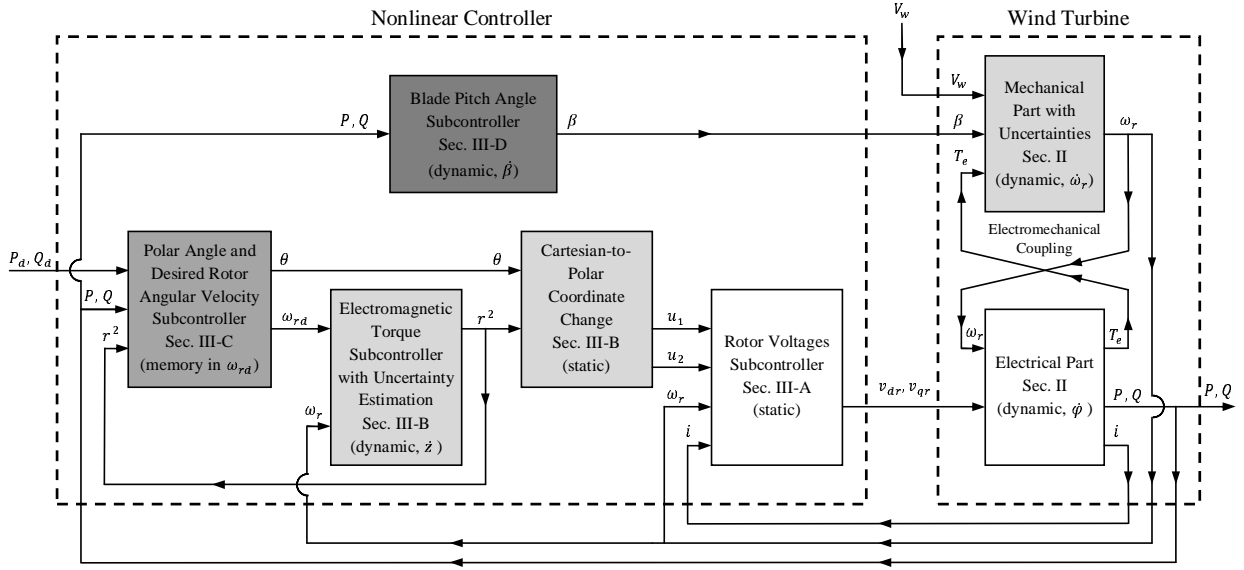


Fig. 1. Model of the wind turbine and architecture of the nonlinear controller.

aerodynamic and mechanical parameters listed at the end of Section II.

To come up with such a subcontroller, we first introduce a coordinate change. As was shown in our previous work [25], because of (2), (7), and (13), the electromagnetic torque T_e may be expressed as a quadratic function of the new control variables u_1 and u_2 , i.e.,

$$T_e = [u_1 \quad u_2] \begin{bmatrix} q_1 & q_2 \\ q_2 & q_3 \end{bmatrix} \begin{bmatrix} u_1 \\ u_2 \end{bmatrix} + [b_1 \quad b_2] \begin{bmatrix} u_1 \\ u_2 \end{bmatrix} + a, \quad (14)$$

where q_1, q_2, q_3, b_1, b_2 , and a depend on the electrical parameters and the state feedback gain matrix K . Moreover, as was shown in [25], this quadratic function is always *convex* because its associated Hessian matrix $\begin{bmatrix} q_1 & q_2 \\ q_2 & q_3 \end{bmatrix}$ is always *positive definite*. Since the mechanical dynamics (6), in ω_r , are driven by T_e , while T_e in (14) is a quadratic function of u_1 and u_2 , the *two* new control variables u_1 and u_2 collectively affect *one* state variable ω_r . This implies that there is a redundancy in u_1 and u_2 , which may be exploited elsewhere. Since the quadratic function is always convex, this redundancy may be exposed via the following coordinate change [25], which transforms $u_1, u_2 \in \mathbb{R}$ in a Cartesian coordinate system into $r \geq 0$ and $\theta \in [-\pi, \pi)$ in a polar coordinate system:

$$r = \sqrt{z_1^2 + z_2^2}, \quad \theta = \text{atan2}(z_2, z_1), \quad (15)$$

where

$$\begin{bmatrix} z_1 \\ z_2 \end{bmatrix} = D^{1/2} M^T \begin{bmatrix} u_1 \\ u_2 \end{bmatrix} + \frac{1}{2} D^{-1/2} M^T \begin{bmatrix} b_1 \\ b_2 \end{bmatrix}, \quad (16)$$

$\text{atan2}(\cdot)$ denotes the four-quadrant arctangent function, and M and D contain the eigenvectors and eigenvalues of $\begin{bmatrix} q_1 & q_2 \\ q_2 & q_3 \end{bmatrix}$ on their columns and diagonal, respectively, i.e., $M^T \begin{bmatrix} q_1 & q_2 \\ q_2 & q_3 \end{bmatrix} M = D$. In the polar coordinates, it follows from (14)–(16) that

$$T_e = r^2 + a', \quad (17)$$

where $a' = -\frac{v_{ds}^2 + v_{qs}^2}{4\omega_s R_s}$ is always negative. From (6) and (17), we see that in the polar coordinates, r^2 is responsible

for driving the mechanical dynamics in ω_r and, hence, may be viewed as an *equivalent electromagnetic torque*, differed from T_e only by a constant a' . On the other hand, the *polar angle* θ has no impact on the mechanical dynamics and, thus, represents the redundancy that will be exploited later, in Section III-C.

Note that (15) and (16) describe the *Cartesian-to-Polar Coordinate Change* block in Figure 1.

Having introduced the coordinate change, we next show that the unknown aerodynamic and mechanical parameters, listed at the end of Section II, can be lumped into a scalar term, simplifying the problem. Combining (6), (8), (9), and (17),

$$J\dot{\omega}_r = \frac{\frac{1}{2}\rho AC_p(\frac{\omega_r R}{V_w}, \beta)V_w^3}{\omega_r} - r^2 - a' - C_f\omega_r. \quad (18)$$

Notice that the unknown parameters—namely, the C_p -surface, the air density ρ , the friction coefficient C_f , and the wind speed V_w —all appear in (18). Moreover, these unknown parameters can be separated from the “control input” r^2 and lumped into a scalar function $g(\omega_r, \beta, V_w)$, defined as

$$g(\omega_r, \beta, V_w) = \frac{\frac{1}{2}\rho AC_p(\frac{\omega_r R}{V_w}, \beta)V_w^3}{\omega_r} - a' - C_f\omega_r. \quad (19)$$

With $g(\omega_r, \beta, V_w)$ in (19) representing the aggregated uncertainties, the first-order dynamics (18) are simplified to

$$\dot{\omega}_r = \frac{1}{J}(g(\omega_r, \beta, V_w) - r^2). \quad (20)$$

To design a controller for r^2 , which allows the rotor angular velocity ω_r to track a desired, slow-varying reference ω_{rd} despite the unknown scalar function $g(\omega_r, \beta, V_w)$, consider a first-order nonlinear system

$$\dot{x} = \frac{1}{J}(f(x) + u), \quad (21)$$

where $x \in \mathbb{R}$ is the state, $u \in \mathbb{R}$ is the input, and $f(x)$ is a *known function* of x . Obviously, to drive x to some desired

value $x_d \in \mathbb{R}$, we may apply feedback linearization [30] to cancel $f(x)$ and insert linear dynamics, i.e., let

$$u = -f(x) - \alpha(x - x_d), \quad (22)$$

where $\alpha \in \mathbb{R}$ is the controller gain. Combining (21) with (22) yields the closed-loop dynamics

$$\dot{x} = -\frac{\alpha}{J}(x - x_d). \quad (23)$$

Thus, if α is positive, x in (23) asymptotically goes to x_d .

Now suppose $f(x)$ in (21) is *unknown* but a *constant*, denoted simply as $f \in \mathbb{R}$ (we will relax the assumption that it is a constant shortly). With f being unknown, the controller (22) is no longer applicable. To overcome this limitation, we may first introduce a reduced-order estimator [32], which calculates an estimate $\hat{f} \in \mathbb{R}$ of f , and then replace $f(x)$ in (22) by the estimate \hat{f} :

$$\dot{z} = -\frac{h}{J}(u + \hat{f}), \quad (24)$$

$$\hat{f} = z + hx, \quad (25)$$

$$u = -\hat{f} - \alpha(x - x_d), \quad (26)$$

where $z \in \mathbb{R}$ is the estimator state and $h \in \mathbb{R}$ is the estimator gain. Defining the estimation error as $\tilde{f} = f - \hat{f}$ and combining (21) with (24)–(26) yield closed-loop dynamics

$$\dot{\tilde{f}} = -\dot{\hat{f}} = -\dot{z} - h\dot{x} = -\frac{h}{J}\tilde{f}, \quad (27)$$

$$\dot{x} = \frac{1}{J}(f - \hat{f} - \alpha(x - x_d)) = \frac{1}{J}(\tilde{f} - \alpha(x - x_d)). \quad (28)$$

Hence, by letting both α and h be positive, both \tilde{f} and x in (27) and (28) asymptotically go to 0 and x_d , respectively.

Next, suppose both the state x and the desired value x_d must be *positive*, instead of being anywhere in \mathbb{R} . With this restriction, the controller with uncertainty estimation (24)–(26) needs to be modified, because for some initial conditions, it is possible that x can become nonpositive. One way to modify the controller is to replace the linear term $x - x_d$ in (26) by a logarithmic one $\ln \frac{x}{x_d}$, resulting in

$$u = -\hat{f} - \alpha \ln \frac{x}{x_d}. \quad (29)$$

With (24), (25), and (29), the closed-loop dynamics become

$$\dot{\tilde{f}} = -\frac{h}{J}\tilde{f}, \quad (30)$$

$$\dot{x} = \frac{1}{J}(\tilde{f} - \alpha \ln \frac{x}{x_d}). \quad (31)$$

Note from (31) that for any $\tilde{f} \in \mathbb{R}$, there exists positive x , sufficiently small, such that \dot{x} is positive. Therefore, for any initial condition $(\tilde{f}(0), x(0))$ with positive $x(0)$, $x(t)$ will remain positive, suggesting that the modification (29) satisfies the restriction.

Now suppose the input u must be *nonpositive*. With this additional restriction, (29) needs to be further modified. One way to do so is to force the right-hand side of (29) to be nonpositive, leading to

$$u = -\max\{\hat{f} + \alpha \ln \frac{x}{x_d}, 0\}. \quad (32)$$

Clearly, with (32), u is always nonpositive.

Finally, suppose f is an *unknown function* of x , denoted as $f(x)$. With this relaxation, we may associate the first-order nonlinear system (21) with the first-order dynamics (20) by viewing x as ω_r , x_d as ω_{rd} , u as $-r^2$, $f(x)$ as $g(\omega_r, \beta, V_w)$ (treating β and V_w as constants), and \hat{f} as \hat{g} (i.e., \hat{g} is an estimate of $g(\omega_r, \beta, V_w)$). Based on this association, (24), (25), and (32) can be written as

$$\dot{z} = -\frac{h}{J}(-r^2 + \hat{g}), \quad (33)$$

$$\hat{g} = z + h\omega_r, \quad (34)$$

$$r^2 = \max\{\hat{g} + \alpha \ln \frac{\omega_r}{\omega_{rd}}, 0\}. \quad (35)$$

Having derived the controller with uncertainty estimation (33)–(35), we now analyze its behavior. To do so, some setup is needed: first, suppose ω_{rd} , β , and V_w are constants. Second, as was shown in [25], because of Assumptions (A1)–(A3) in Section II, there exists $\omega_r^{(1)} \in (0, \infty)$ such that $g(\omega_r^{(1)}, \beta, V_w) = 0$ and $g(\omega_r, \beta, V_w) > 0$ for all $\omega_r \in (0, \omega_r^{(1)})$. Third, using (9), (19), and Assumptions (A1) and (A4), it is straightforward to show that there exist $\underline{\gamma} \in (-\infty, 0)$ and $\overline{\gamma} \in (0, \infty)$ such that $\underline{\gamma} \leq \frac{\partial}{\partial \omega_r} g(\omega_r, \beta, V_w) \leq \overline{\gamma}$ for all $\omega_r \in (0, \infty)$. Finally, with (20) and (33)–(35) and with (ω_r, \hat{g}) as state variables (instead of (ω_r, z)), the closed-loop dynamics can be expressed as

$$\dot{\omega}_r = \frac{1}{J}(g(\omega_r, \beta, V_w) - \max\{\hat{g} + \alpha \ln \frac{\omega_r}{\omega_{rd}}, 0\}), \quad (36)$$

$$\dot{\hat{g}} = \dot{z} + h\dot{\omega}_r = \frac{h}{J}(g(\omega_r, \beta, V_w) - \hat{g}). \quad (37)$$

The following theorem characterizes the stability properties of the closed-loop system (36) and (37):

Theorem 1: Consider the closed-loop system (36) and (37). Suppose ω_{rd} , β , and V_w are constants with $0 < \omega_{rd} \leq \omega_r^{(1)}$, where $\omega_r^{(1)}$, along with $\underline{\gamma}$ and $\overline{\gamma}$, is as defined above. Let $D = \{(\omega_r, \hat{g}) \mid 0 < \omega_r \leq \omega_r^{(1)}, \hat{g} \in \mathbb{R}\} \subset \mathbb{R}^2$. If the controller gain α is positive and the estimator gain h is sufficiently large, i.e.,

$$\begin{aligned} h &> \overline{\gamma} && \text{if } \overline{\gamma} \geq -\frac{1}{3}\underline{\gamma}, \\ h &> -\frac{(\overline{\gamma}-\underline{\gamma})^2}{8(\underline{\gamma}+\overline{\gamma})} && \text{otherwise,} \end{aligned} \quad (38)$$

then: (i) the system has a unique equilibrium point at $(\omega_{rd}, g(\omega_{rd}, \beta, V_w))$ in D ; (ii) the set D is a positively invariant set, i.e., if $(\omega_r(0), \hat{g}(0)) \in D$, then $(\omega_r(t), \hat{g}(t)) \in D \forall t \geq 0$; and (iii) the equilibrium point $(\omega_{rd}, g(\omega_{rd}, \beta, V_w))$ is locally asymptotically stable with a domain of attraction D .

Proof: See the Appendix. ■

Theorem 1 says that, by using the electromagnetic torque subcontroller with uncertainty estimation (33)–(35), if the gains α and h are positive and sufficiently large and if the desired reference ω_{rd} does not exceed $\omega_r^{(1)}$, then the rotor angular velocity ω_r asymptotically converges to ω_{rd} if ω_{rd} , β , and V_w are constants and closely tracks ω_{rd} if they are slow-varying. Notice that the gains α and h can be chosen independently of each other. Also, the condition “ $\omega_{rd} \leq \omega_r^{(1)}$ ” is practically always satisfied, as $\omega_r^{(1)}$ is extremely large [25].

Note that (33)–(35) describe the *Electromagnetic Torque Subcontroller with Uncertainty Estimation* block in Figure 1.

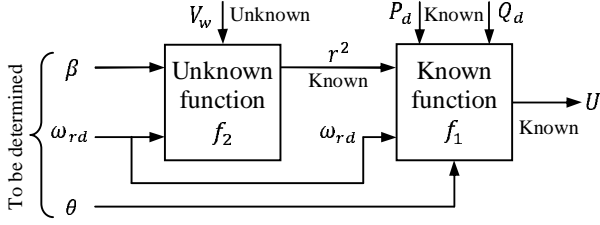


Fig. 2. Relationships among the performance measure U , the to-be-determined variables θ , ω_{rd} , and β , and the exogenous variables V_w , P_d , and Q_d .

C. Polar Angle and Desired Rotor Angular Velocity Subcontroller

Up to this point in the paper, we have yet to specify how θ , ω_{rd} , and β are determined. To do so, we first introduce a scalar performance measure and express this measure as a function of θ , ω_{rd} , and β . We then present a method for choosing these variables, which optimizes the measure.

Recall that the ultimate goal is to make the active and reactive powers P and Q track some desired references P_d and Q_d as closely as possible. Hence, it is useful to introduce a scalar performance measure, which characterizes how far P and Q are from P_d and Q_d . One such measure, denoted as U , is given by

$$U = \frac{1}{2} [P - P_d \quad Q - Q_d] \begin{bmatrix} w_p & w_{pq} \\ w_{pq} & w_q \end{bmatrix} \begin{bmatrix} P - P_d \\ Q - Q_d \end{bmatrix}, \quad (39)$$

where w_p , w_q , and w_{pq} are design parameters satisfying $w_p > 0$ and $w_p w_q > w_{pq}^2$, so that $\begin{bmatrix} w_p & w_{pq} \\ w_{pq} & w_q \end{bmatrix}$ is a positive definite matrix. With these design parameters, one may specify how the differences $P - P_d$ and $Q - Q_d$ and their product $(P - P_d)(Q - Q_d)$ are penalized. Moreover, with U in (39) being a quadratic, positive definite function of $P - P_d$ and $Q - Q_d$, the smaller U is, the better the ultimate goal is achieved.

Having defined the performance measure U via (39), we next establish the following statement: if the subcontrollers in Sections III-A and III-B are used with K chosen so that $A - BK$ has very fast eigenvalues, α chosen to be positive, and h chosen to satisfy (38), and if θ , ω_{rd} , β , V_w , P_d , and Q_d are all constants, then after a short transient, U may be expressed as a *known* function f_1 of r^2 , θ , ω_{rd} , P_d , and Q_d , while r^2 , in turn, may be expressed as an *unknown* function f_2 of ω_{rd} , β , and V_w , i.e.,

$$U = f_1(r^2, \theta, \omega_{rd}, P_d, Q_d), \quad (40)$$

$$r^2 = f_2(\omega_{rd}, \beta, V_w), \quad (41)$$

as shown in Figure 2. To establish this statement, suppose the hypothesis is true. Then, after a short transient, it follows from (39) that U is a known function of P , Q , P_d , and Q_d ; from (2), (3)–(5), (10), and (11) that P and Q are known functions of φ , ω_r , u_1 , and u_2 ; from (13) that φ is a known function of u_1 and u_2 ; from (15) and (16) that u_1 and u_2 are known functions of r^2 and θ ; and from Theorem 1 that $\omega_r = \omega_{rd}$. Thus, (40) holds with f_1 being known. On the other hand, it follows from (35) and Theorem 1 that $r^2 = g(\omega_{rd}, \beta, V_w)$. Hence, (41) holds with f_2 being unknown.

Equations (40) and (41), which are represented in Figure 2, suggest that U is a function of the to-be-determined variables θ , ω_{rd} , and β as well as the exogenous variables V_w , P_d , and Q_d . Given that the smaller U is the better, these to-be-determined variables may be chosen to minimize U . However, such minimization is difficult to carry out because although P_d and Q_d are known, V_w is not. To make matter worse, since f_1 is known but f_2 is not, the objective function is not entirely known. Somewhat fortunately, as was shown in Figure 2, θ affects U only through f_1 and not f_2 . Therefore, θ may be chosen to minimize U for any given r^2 , ω_{rd} , P_d , and Q_d , i.e.,

$$\theta = \arg \min_{x \in [-\pi, \pi]} f_1(r^2, x, \omega_{rd}, P_d, Q_d), \quad (42)$$

which is implementable since r^2 , ω_{rd} , P_d , and Q_d are all known. With θ chosen as in (42), the minimization problem reduces from a three-dimensional problem to a two-dimensional one, depending only on ω_{rd} and β . Since the objective function upon absorbing θ is unknown and since V_w may change quickly, instead of minimizing U with respect to both ω_{rd} and β —which may take a long time—we decide to sacrifice freedom for speed, minimizing U only with respect to ω_{rd} and updating β in a relatively slower fashion, which will be described in Section III-D.

The minimization of U with respect to ω_{rd} is carried out based on a gradient-like approach as shown in Figure 3. To explain the rationale behind this approach, suppose β , V_w , P_d , and Q_d are constants. Then, according to (40)–(42), U is an unknown function of ω_{rd} . Because this function is not known, its gradient $\frac{\partial U}{\partial \omega_{rd}}$ at any ω_{rd} cannot be evaluated. To alleviate this issue, we evaluate U at two nearby ω_{rd} 's, use the two evaluated U 's to obtain an estimate of the gradient $\frac{\partial U}{\partial \omega_{rd}}$, and move ω_{rd} along the direction where U decreases, by an amount which depends on the gradient estimate. This idea is illustrated in Figure 3 and described precisely as follows: the desired rotor angular velocity $\omega_{rd}(t)$ is set to an initial value $\omega_{rd}(0)$ at time $t = 0$ and held constant until $t = T_1$, where T_1 should be sufficiently large so that both the electrical and mechanical dynamics have a chance to reach steady-state, but not too large which causes the minimization to be too slow. From time $t = T_1 - T_0$ to $t = T_1$, the average of $U(t)$, i.e., $\frac{1}{T_0} \int_{T_1 - T_0}^{T_1} U(t) dt$, is recorded as the first value needed to obtain a gradient estimate. Similar to T_1 , T_0 should be large enough so that small fluctuations in $U(t)$ (induced perhaps by a noisy V_w) are averaged out, but not too large which causes transient in the dynamics to be included. The variable $\omega_{rd}(t)$ is then changed gradually in an S-shape manner from $\omega_{rd}(0)$ at time $t = T_1$ to a nearby $\omega_{rd}(0) + \Delta\omega_{rd}(T_1)$ at $t = T_1 + T_2$, where $\Delta\omega_{rd}(T_1)$ is an initial stepsize, and T_2 should be sufficiently large but not overly so, so that the transition in $\omega_{rd}(t)$ is smooth and yet not too slow. The variable $\omega_{rd}(t)$ is then held constant until $t = 2T_1 + T_2$, and the average of $U(t)$ from $t = 2T_1 + T_2 - T_0$ to $t = 2T_1 + T_2$, i.e., $\frac{1}{T_0} \int_{2T_1 + T_2 - T_0}^{2T_1 + T_2} U(t) dt$, is recorded as the second value needed to obtain the gradient estimate. At time $t = 2T_1 + T_2$, the two recorded values are used to form the gradient estimate, which is in turn used to decide a new stepsize $\Delta\omega_{rd}(2T_1 + T_2)$

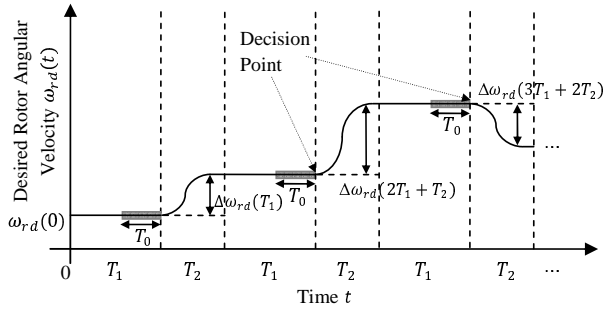


Fig. 3. A graphical illustration of the gradient-like approach.

through

$$\Delta\omega_{rd}(2T_1 + T_2) = -\epsilon_1 \text{sat} \left(\frac{\frac{1}{T_0} \int_{2T_1+T_2-T_0}^{2T_1+T_2} U(t)dt - \frac{1}{T_0} \int_{T_1-T_0}^{T_1} U(t)dt}{\epsilon_2 \Delta\omega_{rd}(T_1)} \right), \quad (43)$$

where $\epsilon_1 > 0$ and $\epsilon_2 > 0$ are design parameters that define the new stepsize $\Delta\omega_{rd}(2T_1 + T_2)$, and $\text{sat}()$ denotes the standard saturation function that limits $\Delta\omega_{rd}(2T_1 + T_2)$ to $\pm\epsilon_1$. Upon deciding $\Delta\omega_{rd}(2T_1 + T_2)$, $\omega_{rd}(t)$ is again changed in an S-shape manner from $\omega_{rd}(0) + \Delta\omega_{rd}(T_1)$ at $t = 2T_1 + T_2$ to $\omega_{rd}(0) + \Delta\omega_{rd}(T_1) + \Delta\omega_{rd}(2T_1 + T_2)$ at $t = 2T_1 + 2T_2$, in a way similar to the time interval $[T_1, T_1 + T_2]$. The process then repeats with the second recorded value from the previous cycle $[0, 2T_1 + T_2]$ becoming the first recorded value for the next cycle $[T_1 + T_2, 3T_1 + 2T_2]$, and so on. Therefore, with this gradient-like approach, ω_{rd} is guaranteed to approach a local minimum when β , V_w , P_d , and Q_d are constants, and track a local minimum when they are slow-varying.

Note that (39), (42), and (43) describe the *Polar Angle and Desired Rotor Angular Velocity Subcontroller* block in Figure 1.

D. Blade Pitch Angle Subcontroller

As was mentioned, in order to speed up the minimization, we have decided to minimize U only with respect to ω_{rd} , leaving the blade pitch angle β as the remaining undetermined variable. Given that an active power P that is larger than the rated value P_{rated} of the turbine may cause damage, we decide to use β to prevent P from exceeding P_{rated} , thereby protecting the turbine. Specifically, we let β be updated according to

$$\dot{\beta} = \begin{cases} 0 & \text{if } \beta = \beta_{\min} \text{ and } P < P_{\text{rated}}, \\ 0 & \text{if } \beta = \beta_{\max} \text{ and } P > P_{\text{rated}}, \\ -\epsilon_3(P_{\text{rated}} - P) & \text{otherwise,} \end{cases} \quad (44)$$

where $\epsilon_3 > 0$ is a design parameter that dictates the rate at which β changes. Note that with (44), β is guaranteed to lie between β_{\min} and β_{\max} . Moreover, when P is above (below) P_{rated} , β increases (decreases) if possible, in order to try to capture less (more) wind power, which leads to a smaller (larger) P .

Note that (44) describes the *Blade Pitch Angle Subcontroller* block in Figure 1.

Remark 1: The blade pitch angle subcontroller may be designed based on other considerations. For example, if the forecast of, say, the hourly-average wind speed \bar{V}_w is available, for blade protection β may be chosen as $\beta = F(\bar{V}_w)$ for some non-decreasing function $F : (0, \infty) \rightarrow [\beta_{\min}, \beta_{\max}]$.

IV. SIMULATION RESULTS

To demonstrate the capability and effectiveness of the proposed controller, simulation has been carried out in MATLAB. To describe the simulation settings and results, both the per-unit and physical unit systems will be used interchangeably.

The simulation settings are as follows: we consider a 1.5 MW, 575 V, 60 Hz wind turbine that is essentially adopted from the Distributed Resources Library in MATLAB/Simulink R2007a. The values of the wind turbine parameters are: $\omega_s = 1$ pu, $R_s = 0.00706$ pu, $R_r = 0.005$ pu, $L_s = 3.071$ pu, $L_r = 3.056$ pu, $L_m = 2.9$ pu, $v_{ds} = 1$ pu, $v_{qs} = 0$ pu, $J = 10.08$ pu, $A = 4656.6$ m², $R = 38.5$ m, $\beta_{\min} = 0$ deg, $\beta_{\max} = 30$ deg, and $C_f = 0.01$ pu. The C_p -surface adopted by MATLAB, which is taken from [33], is $C_p(\lambda, \beta) = c_1 \left(\frac{c_2}{\lambda_i} - c_3\beta - c_4 \right) e^{-\frac{c_5}{\lambda_i}} + c_6\lambda$, where $\frac{1}{\lambda_i} = \frac{1}{\lambda + 0.08\beta} - \frac{0.035}{\beta^3 + 1}$, $c_1 = 0.5176$, $c_2 = 116$, $c_3 = 0.4$, $c_4 = 5$, $c_5 = 21$, and $c_6 = 0.0068$. The mechanical power captured by the wind turbine is $P_m(\text{pu}) = \frac{P_{\text{nom}} P_{\text{wind_base}}}{P_{\text{elec_base}}} C_p(\text{pu}) V_w(\text{pu})^3$, where $P_m(\text{pu}) = \frac{P_m}{P_{\text{nom}}}$, $P_{\text{nom}} = 1.5$ MW is the nominal mechanical power, $P_{\text{wind_base}} = 0.73$ pu is the maximum power at the base wind speed, $P_{\text{elec_base}} = 1.5 \times 10^6 / 0.9$ VA is the base power of the electrical generator, $C_p(\text{pu}) = \frac{C_p}{C_{p_nom}}$, $C_{p_nom} = 0.48$ is the peak of the C_p -surface, $V_w(\text{pu}) = \frac{V_w}{V_{w_base}}$, and $V_{w_base} = 12$ m/s is the base wind speed. Note that the maximum mechanical power, captured at the base wind speed, is 0.657 pu. The tip speed ratio is $\lambda(\text{pu}) = \frac{\omega_r(\text{pu})}{V_w(\text{pu})}$, where $\lambda(\text{pu}) = \frac{\lambda}{\lambda_{\text{nom}}}$, $\lambda_{\text{nom}} = 8.1$ is the λ that yields the peak of the C_p -surface, $\omega_{r_base} = 1.2$ pu is the base rotational speed, $\omega_r(\text{pu}) = \frac{\omega_r}{\omega_{r_nom}}$, and $\omega_{r_nom} = 2.1039$ rad/sec is the nominal rotor angular velocity. For more details on these parameters and values, see the MATLAB documentation.

As for the proposed controller, we choose its parameters as follows: for the Rotor Voltages Subcontroller, we let the desired closed-loop eigenvalues of the electrical dynamics be at -10 , -15 , and $-20 \pm 5j$. Using MATLAB's `place()` function, the state feedback gain matrix $K = [K_1 \ K_2]^T$ that yields these eigenvalues is found to be $K_1 = [12277 \ -4493.8 \ 32.7 \ -6.3]^T$ and $K_2 = [-1615.4 \ 12117 \ -0.4 \ 32.2]^T$. Moreover, we let $\alpha = 5$ and $h = 16$ for the Electromagnetic Torque Subcontroller with Uncertainty Estimation; $w_p = 10$, $w_q = 1$, $w_{pq} = 0$, $\epsilon_1 = 0.025$, $\epsilon_2 = 2$, $T_0 = 1$ s, $T_1 = 4$ s, and $T_2 = 6$ s for the Polar Angle and Desired Rotor Angular Velocity Subcontroller; and $\epsilon_3 = 2.7$ and $P_{\text{rated}} = 1$ pu for the Blade Pitch Angle Subcontroller.

The simulation results are as follows: we consider a scenario where the wind speed V_w is derived from an actual wind profile from a wind farm located in northwest Oklahoma, the desired active power P_d experiences large step changes between 0.3 pu and 1 pu, and the desired reactive power Q_d

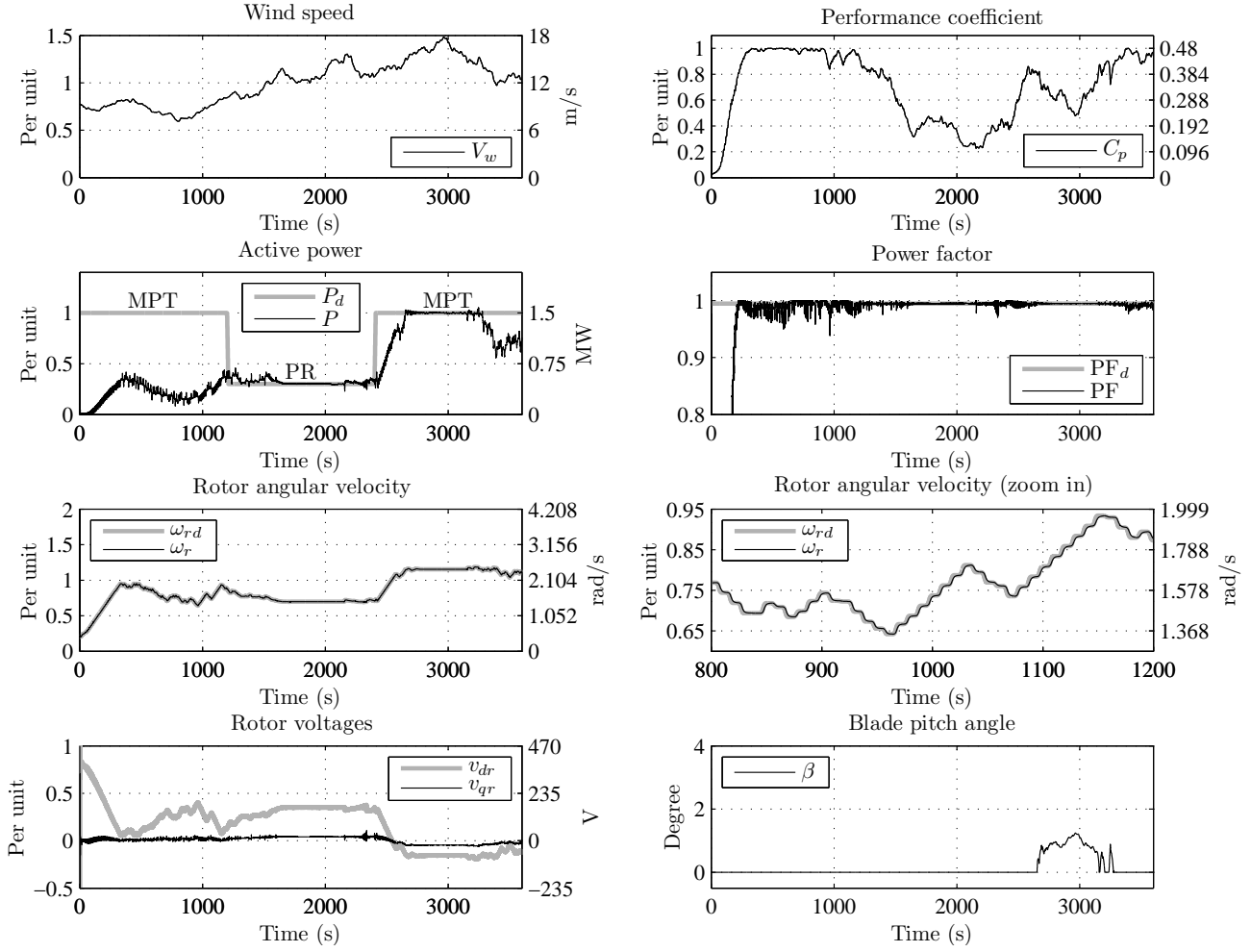


Fig. 4. Effective operation in both the MPT and PR modes and seamless switching between them under an actual wind profile from a wind farm located in northwest Oklahoma.

is such that the desired power factor PF_d is fixed at 0.995. As will be explained below, these values force the turbine to operate in both the MPT and PR modes, along with switching between them, under a realistic wind profile. Figure 4 shows the simulation results for this scenario in both the per-unit and physical unit systems, wherever applicable. Subplot 1 shows the wind profile V_w . Subplot 2 shows the value of C_p , while subplot 3 shows the desired and actual active powers P_d and P . Note that, for the first 1200 seconds during which P_d is unachievable at 1 pu, the turbine operates in the MPT mode and maximizes P , as indicated by the value of C_p approaching its maximum of 0.48 after a short transient (the turbine is initially at rest). At time 1200s when P_d drops sharply from 1 pu to an achievable value of 0.3 pu, the turbine quickly reduces the value of C_p , accurately regulates P around P_d , and effectively rejects the “disturbance” V_w , thereby smoothly switches from the MPT mode to the PR mode. At time 2400s when P_d goes from 0.3 pu back to 1 pu, the MPT mode resumes. Because V_w is strong enough at that time, P approaches P_d . Moreover, the moment P exceeds P_d (which is equal to P_{rated}), the blade pitch angle β increases as shown in subplot 8 in order to clip the power and protect the

turbine. At time 3275s when V_w becomes weaker, β returns to $\beta_{min} = 0$ deg, thereby allowing the value of C_p to return to its maximum of 0.48 and P to be maximized. Subplot 4 shows the desired and actual power factors PF_d and PF , while subplots 5 and 6 show the desired and actual rotor angular velocities ω_{rd} and ω_r in normal and zoomed-in views. As can be seen from these subplots, throughout the simulation, both PF and ω_r are maintained near PF_d and ω_{rd} , respectively, affected only slightly by the random wind fluctuations. Moreover, the small S-shape variations in ω_{rd} in subplot 6 resemble those in Figure 3. Finally, subplots 7 and 8 show the control variables, i.e., the rotor voltages v_{dr} and v_{qr} as well as the blade pitch angle β .

The above simulation results suggest that the proposed controller not only is capable of operating effectively in both the MPT and PR modes, it is also capable of switching smoothly between them—all while not knowing the C_p -surface, air density, friction coefficient, and wind speed.

V. CONCLUDING REMARKS

In this paper, we have designed a controller for a variable-speed wind turbine with a DFIG. The controller, consisting

of four subcontrollers, has been developed based on a fifth-order, electromechanically-coupled, nonlinear model of the wind turbine by integrating several linear and nonlinear control strategies and exploiting time-scale separation in the dynamics. We have shown that the controller is able to make the wind turbine operate in both the MPT and PR modes and switch smoothly between them, in addition to maintaining a desired power factor. Furthermore, the controller does not require knowledge of the C_p -surface, air density, friction coefficient, and wind speed. Simulation has been carried out using a realistic wind profile, and the results demonstrate the capability and effectiveness of the controller. Future work includes designing a comprehensive wind farm controller for a multitude of turbines, which builds upon results documented in this paper.

APPENDIX PROOF OF THEOREM 1

First, we show (i). Setting $\dot{\omega}_r$ and $\dot{\hat{g}}$ in (36) and (37) to zero yields $g(\omega_r, \beta, V_w) = \max\{\hat{g} + \alpha \ln \frac{\omega_r}{\omega_{rd}}, 0\}$ and $\hat{g} = g(\omega_r, \beta, V_w)$. When $\hat{g} + \alpha \ln \frac{\omega_r}{\omega_{rd}} \geq 0$, we have $\omega_r = \omega_{rd}$ and $\hat{g} = g(\omega_{rd}, \beta, V_w)$. Thus, $(\omega_{rd}, g(\omega_{rd}, \beta, V_w))$ is an equilibrium point, which is in D , since $0 < \omega_{rd} \leq \omega_r^{(1)}$. On the other hand, when $\hat{g} + \alpha \ln \frac{\omega_r}{\omega_{rd}} < 0$, we have $\omega_r \in \Omega$ and $\hat{g} = 0$, where $\Omega = \{\omega \in (0, \infty) : g(\omega, \beta, V_w) = 0\}$ and $\omega_r^{(1)} = \min \Omega$. Since $\hat{g} + \alpha \ln \frac{\omega_r}{\omega_{rd}} < 0$ and $\hat{g} = 0$, we have $\omega_r < \omega_{rd}$. Since $\omega_r \in \Omega$, $\omega_r^{(1)} = \min \Omega$, and $\omega_{rd} \leq \omega_r^{(1)}$, we have $\omega_r \geq \omega_{rd}$. Hence, there is a contradiction, implying that when $\hat{g} + \alpha \ln \frac{\omega_r}{\omega_{rd}} < 0$, there is no equilibrium point in D . This proves (i).

Next, we show (ii). To do so, it is useful to think of D as a vertical strip in the two-dimensional state space (ω_r, \hat{g}) . Notice that on the right boundary of the strip where $\omega_r = \omega_r^{(1)}$, because of (36) and because $g(\omega_r^{(1)}, \beta, V_w) = 0$ and $\max\{\hat{g} + \alpha \ln \frac{\omega_r^{(1)}}{\omega_{rd}}, 0\} \geq 0$, we have $\dot{\omega}_r \leq 0$. Thus, the state (ω_r, \hat{g}) cannot escape D through the right boundary. Next, note that for each fixed $\hat{g} \in \mathbb{R}$, there exists $\omega_r^* > 0$ such that for all $\omega_r \in (0, \omega_r^*)$, $\hat{g} + \alpha \ln \frac{\omega_r}{\omega_{rd}} < 0$. This, along with (36) and the fact that $g(\omega, \beta, V_w) > 0$ for all $\omega \in (0, \omega_r^{(1)})$, implies that near the left boundary of the strip where ω_r is arbitrarily small but positive, we have $\dot{\omega}_r > 0$. Hence, the state (ω_r, \hat{g}) cannot escape D through the left boundary. This proves (ii).

Finally, we show (iii). Consider a Lyapunov function candidate $V : D \rightarrow \mathbb{R}$, defined as $V(\omega_r, \hat{g}) = \alpha c(\omega_r \ln \frac{\omega_r}{\omega_{rd}} - \omega_r + \omega_{rd}) + \frac{1}{2}(g(\omega_r, \beta, V_w) - \hat{g})^2$, where $c > 0$ is to be determined. Note that V is continuously differentiable over D . Moreover, V is positive definite over D with respect to the equilibrium point $(\omega_{rd}, g(\omega_{rd}, \beta, V_w))$, since $V(\omega_{rd}, g(\omega_{rd}, \beta, V_w)) = 0$ and $V(\omega_r, \hat{g}) > 0$ for all $(\omega_r, \hat{g}) \neq (\omega_{rd}, g(\omega_{rd}, \beta, V_w))$ due to the property $\omega_r \ln \frac{\omega_r}{\omega_{rd}} - \omega_r + \omega_{rd} > 0$ for all $\omega_r \neq \omega_{rd}$. Furthermore, V is unbounded toward the top, bottom, and left boundary of the vertical strip D , but not so toward the right boundary of D . This is because for each fixed $\omega_r \in (0, \omega_r^{(1)})$, $\lim_{|\hat{g}| \rightarrow \infty} V(\omega_r, \hat{g}) = \infty$, and for each fixed $\hat{g} \in \mathbb{R}$, $\lim_{\omega_r \rightarrow 0} V(\omega_r, \hat{g}) = \infty$ and $V(\omega_r^{(1)}, \hat{g}) < \infty$. Note that although V is not unbounded toward the right boundary of D , the state (ω_r, \hat{g}) cannot cross this boundary due to (ii).

Differentiating V and using (36) and (37), we get

$$J\dot{V} = \begin{bmatrix} \alpha c \ln \frac{\omega_r}{\omega_{rd}} + (g - \hat{g}) \frac{\partial g}{\partial \omega_r} \\ -(g - \hat{g}) \end{bmatrix}^T \begin{bmatrix} g - \max\{\hat{g} + \alpha \ln \frac{\omega_r}{\omega_{rd}}, 0\} \\ h(g - \hat{g}) \end{bmatrix},$$

where, for convenience, the function arguments are omitted. Note that because of (ii) and the above properties of V , to show (iii), it suffices to show that \dot{V} is negative definite over D with respect to the equilibrium point $(\omega_{rd}, g(\omega_{rd}, \beta, V_w))$. To this end, let D be partitioned into two disjoint sets $D_1 = \{(\omega_r, \hat{g}) \in D : \hat{g} + \alpha \ln \frac{\omega_r}{\omega_{rd}} \geq 0\}$ and $D_2 = \{(\omega_r, \hat{g}) \in D : \hat{g} + \alpha \ln \frac{\omega_r}{\omega_{rd}} < 0\}$. Note that the equilibrium point $(\omega_{rd}, g(\omega_{rd}, \beta, V_w))$ is in D_1 .

Suppose $(\omega_r, \hat{g}) \in D_1$. Then, \dot{V} takes a quadratic form:

$$J\dot{V} = - \begin{bmatrix} \ln \frac{\omega_r}{\omega_{rd}} \\ g - \hat{g} \end{bmatrix}^T \begin{bmatrix} \alpha^2 c & \frac{\alpha}{2} (\frac{\partial g}{\partial \omega_r} - c) \\ \frac{\alpha}{2} (\frac{\partial g}{\partial \omega_r} - c) & h - \frac{\partial g}{\partial \omega_r} \end{bmatrix} \begin{bmatrix} \ln \frac{\omega_r}{\omega_{rd}} \\ g - \hat{g} \end{bmatrix}.$$

Note that if $(\omega_r, \hat{g}) = (\omega_{rd}, g(\omega_{rd}, \beta, V_w))$, $\dot{V} = 0$. Also, the leading principal minors of the above symmetric matrix are $\alpha^2 c$ and $\alpha^2 c(h - \frac{1}{4c}(\frac{\partial g}{\partial \omega_r} + c)^2)$. Thus, if h and c satisfy

$$h - \frac{1}{4c}(\frac{\partial}{\partial \omega} g(\omega, \beta, V_w) + c)^2 > 0, \quad \forall \omega \in (0, \infty), \quad (45)$$

then this symmetric matrix is positive definite, so that $\dot{V} < 0$ for any $(\omega_r, \hat{g}) \neq (\omega_{rd}, g(\omega_{rd}, \beta, V_w))$. Therefore, if h and c satisfy (45), \dot{V} is negative definite over D_1 with respect to $(\omega_{rd}, g(\omega_{rd}, \beta, V_w))$.

Next, suppose $(\omega_r, \hat{g}) \in D_2$. Then, \dot{V} is bounded from above by a quadratic form:

$$\begin{aligned} J\dot{V} &= -h\hat{g}^2 + (2h - \frac{\partial g}{\partial \omega_r})g\hat{g} + (\frac{\partial g}{\partial \omega_r} - h)g^2 + \alpha c g \ln \frac{\omega_r}{\omega_{rd}} \\ &\leq -h\hat{g}^2 + (2h - \frac{\partial g}{\partial \omega_r})g\hat{g} + (\frac{\partial g}{\partial \omega_r} - h)g^2 - cg\hat{g} \\ &= - \begin{bmatrix} \hat{g} \\ g \end{bmatrix}^T \begin{bmatrix} h & \frac{1}{2}(\frac{\partial g}{\partial \omega_r} + c - 2h) \\ \frac{1}{2}(\frac{\partial g}{\partial \omega_r} + c - 2h) & h - \frac{\partial g}{\partial \omega_r} \end{bmatrix} \begin{bmatrix} \hat{g} \\ g \end{bmatrix}. \end{aligned}$$

Note that the leading principal minors of the above symmetric matrix are h and $c(h - \frac{1}{4c}(\frac{\partial g}{\partial \omega_r} + c)^2)$. Thus, if h and c satisfy (45), then this symmetric matrix is positive definite. Since $(\omega_r, \hat{g}) \in D_2$ and $\omega_{rd} \leq \omega_r^{(1)}$, if $\hat{g} = 0$, then $g > 0$. Thus, \hat{g} and g cannot be zero simultaneously. Hence, $\dot{V} < 0$. Therefore, if h and c satisfy (45), \dot{V} is negative over D_2 .

As it follows from the above, if h and c satisfy (45), \dot{V} is negative definite over D with respect to the equilibrium point $(\omega_{rd}, g(\omega_{rd}, \beta, V_w))$, so that (iii) holds.

It remains to show that if h satisfies (38), then there exists $c > 0$ such that (45) holds. Suppose h satisfies (38). Let $F(\underline{\gamma}, \bar{\gamma}) = \bar{\gamma}$ if $\bar{\gamma} \geq -\frac{1}{3}\underline{\gamma}$ and $F(\underline{\gamma}, \bar{\gamma}) = -\frac{(\bar{\gamma}-\underline{\gamma})^2}{8(\underline{\gamma}+\bar{\gamma})}$ otherwise. Then, $h > F(\underline{\gamma}, \bar{\gamma})$. Let $f(x, \underline{\gamma}, \bar{\gamma}) = \frac{1}{4x} \max\{(\underline{\gamma} + x)^2, (\bar{\gamma} + x)^2\}$, where $x > 0$. Then, it can be shown that $F(\underline{\gamma}, \bar{\gamma}) = \min_{x>0} f(x, \underline{\gamma}, \bar{\gamma})$ by considering the following three cases separately: $\bar{\gamma} \geq -\underline{\gamma}$, $-\underline{\gamma} > \bar{\gamma} \geq -\frac{1}{3}\underline{\gamma}$, and $-\frac{1}{3}\underline{\gamma} > \bar{\gamma}$. Because $h > F(\underline{\gamma}, \bar{\gamma})$, there exists $c > 0$, given by $c = \arg \min_{x>0} f(x, \underline{\gamma}, \bar{\gamma})$, such that $h > f(c, \underline{\gamma}, \bar{\gamma})$. Because $\underline{\gamma} \leq \frac{\partial}{\partial \omega} g(\omega, \beta, V_w) \leq \bar{\gamma}$ for all $\omega \in (0, \infty)$ and by definition of $f(x, \underline{\gamma}, \bar{\gamma})$, we have $\frac{1}{4c}(\frac{\partial}{\partial \omega} g(\omega, \beta, V_w) + c)^2 \leq f(c, \underline{\gamma}, \bar{\gamma})$ for all $\omega \in (0, \infty)$. Since $h > f(c, \underline{\gamma}, \bar{\gamma})$, (45) holds, as desired.

REFERENCES

- [1] "Interim report—system disturbance on 4 November 2006," Union for the Co-Ordination of Transmission of Electricity, Brussels, Belgium, Executive Summary, 2006.
- [2] "European Wind Turbine Testing Procedure Development," Riso National Laboratory, Roskilde, Denmark, Tech. Rep., 2001.
- [3] "Controls Advanced Research Turbine (CART) Commissioning and Baseline Data Collection," National Renewable Energy Laboratory, Golden, CO, Tech. Rep., 2002.
- [4] E. Iyasere, M. Salah, D. Dawson, and J. Wagner, "Nonlinear robust control to maximize energy capture in a variable speed wind turbine," in *Proc. American Control Conference*, Seattle, WA, 2008, pp. 1824–1829.
- [5] K. E. Johnson, L. J. Fingersh, M. J. Balas, and L. Y. Pao, "Methods for increasing region 2 power capture on a variable-speed wind turbine," *Journal of Solar Energy Engineering*, vol. 126, no. 4, pp. 1092–1100, 2004.
- [6] K. E. Johnson, L. Y. Pao, M. J. Balas, and L. J. Fingersh, "Control of variable-speed wind turbines: standard and adaptive techniques for maximizing energy capture," *IEEE Control Systems Magazine*, vol. 26, no. 3, pp. 70–81, 2006.
- [7] V. Galdi, A. Piccolo, and P. Siano, "Designing an adaptive fuzzy controller for maximum wind energy extraction," *IEEE Transactions on Energy Conversion*, vol. 23, no. 2, pp. 559–569, 2008.
- [8] R. B. Chedid, S. H. Karaki, and C. El-Chamali, "Adaptive fuzzy control for wind-diesel weak power systems," *IEEE Transactions on Energy Conversion*, vol. 15, no. 1, pp. 71–78, 2000.
- [9] B. Beltran, T. Ahmed-Ali, and M. E. H. Benbouzid, "Sliding mode power control of variable-speed wind energy conversion systems," *IEEE Transactions on Energy Conversion*, vol. 23, no. 2, pp. 551–558, 2008.
- [10] H. Geng and G. Yang, "Robust pitch controller for output power levelling of variable-speed variable-pitch wind turbine generator systems," *IET Renewable Power Generation*, vol. 3, no. 2, pp. 168–179, 2009.
- [11] E. Muljadi and C. P. Butterfield, "Pitch-controlled variable-speed wind turbine generation," *IEEE Transactions on Industry Applications*, vol. 37, no. 1, pp. 240–246, 2001.
- [12] T. Senjyu, R. Sakamoto, N. Urasaki, T. Funabashi, H. Fujita, and H. Sekine, "Output power leveling of wind turbine generator for all operating regions by pitch angle control," *IEEE Transactions on Energy Conversion*, vol. 21, no. 2, pp. 467–475, 2006.
- [13] K. Stol and M. J. Balas, "Full-state feedback control of a variable-speed wind turbine: A comparison of periodic and constant gains," *Journal of Solar Energy Engineering*, vol. 123, no. 4, pp. 319–326, 2001.
- [14] A. D. Wright and M. J. Balas, "Design of state-space-based control algorithms for wind turbine speed regulation," *Journal of Solar Energy Engineering*, vol. 125, no. 4, pp. 386–395, 2003.
- [15] G. C. Tarnowski and R. Reginatto, "Adding active power regulation to wind farms with variable speed induction generators," in *Proc. IEEE Power Engineering Society General Meeting*, Tampa, FL, 2007, pp. 1–8.
- [16] H.-S. Ko, G.-G. Yoon, and W.-P. Hong, "Active use of DFIG-based variable-speed wind-turbine for voltage regulation at a remote location," *IEEE Transactions on Power Systems*, vol. 22, no. 4, pp. 1916–1925, 2007.
- [17] B. Marinescu, "A robust coordinated control of the doubly-fed induction machine for wind turbines: a state-space based approach," in *Proc. American Control Conference*, Boston, MA, 2004, pp. 174–179.
- [18] D. Zhi and L. Xu, "Direct power control of DFIG with constant switching frequency and improved transient performance," *IEEE Transactions on Energy Conversion*, vol. 22, no. 1, pp. 110–118, 2007.
- [19] F. Wu, X. Zhang, P. Ju, and M. J. H. Sterling, "Decentralized nonlinear control of wind turbine with doubly fed induction generator," *IEEE Transactions on Power Systems*, vol. 23, no. 2, pp. 613–621, 2008.
- [20] R. Pena, J. C. Clare, and G. M. Asher, "Doubly fed induction generator using back-to-back PWM converters and its application to variable-speed wind-energy generation," *IEE Proc. Electric Power Applications*, vol. 143, no. 3, pp. 231–241, 1996.
- [21] B. Hopfensperger, D. J. Atkinson, and R. A. Lakin, "Stator-flux-oriented control of a doubly-fed induction machine with and without position encoder," *IEE Proc. Electric Power Applications*, vol. 147, no. 4, pp. 241–250, 2000.
- [22] A. Monroy, L. Alvarez-Icaza, and G. Espinosa-Perez, "Passivity-based control for variable speed constant frequency operation of a DFIG wind turbine," *International Journal of Control*, vol. 81, no. 9, pp. 1399–1407, 2008.
- [23] S. Peresada, A. Tilli, and A. Tonielli, "Power control of a doubly fed induction machine via output feedback," *Control Engineering Practice*, vol. 12, pp. 41–57, 2004.
- [24] A. D. Hansen, P. Sorensen, F. Iov, and F. Blaabjerg, "Control of variable speed wind turbines with doubly-fed induction generators," *Wind Engineering*, vol. 28, no. 4, pp. 411–434, 2004.
- [25] C. Y. Tang, Y. Guo, and J. N. Jiang, "Nonlinear Dual-Mode Control of Variable-Speed Wind Turbines with Doubly Fed Induction Generators," *IEEE Transactions on Control Systems Technology*, 2010, accepted.
- [26] B. K. Bose, *Modern Power Electronics and AC Drives*. Upper Saddle River, NJ: Prentice Hall PTR, 2002.
- [27] R. Fadaeinedjad, M. Moallem, and G. Moschopoulos, "Simulation of a wind turbine with doubly-fed induction generator by FAST and Simulink," *IEEE Transactions on Energy Conversion*, vol. 23, no. 2, pp. 690–700, 2008.
- [28] Y. Lei, A. Mullane, G. Lightbody, and R. Yacamini, "Modeling of the wind turbine with a doubly fed induction generator for grid integration studies," *IEEE Transactions on Energy Conversion*, vol. 21, no. 1, pp. 257–264, 2006.
- [29] F. D. Bianchi, H. De Battista, and R. J. Mantz, *Wind Turbine Control Systems: Principles, Modelling, and Gain Scheduling Design*. London, England: Springer, 2007.
- [30] H. K. Khalil, *Nonlinear Systems*, 3rd ed. Upper Saddle River, NJ: Prentice Hall, 2001.
- [31] C.-T. Chen, *Linear System Theory and Design*, 3rd ed. New York, NY: Oxford University Press, 1999.
- [32] W. L. Brogan, *Modern Control Theory*, 3rd ed. Englewood Cliffs, NJ: Prentice Hall, 1991.
- [33] S. Heier, *Grid Integration of Wind Energy Conversion Systems*. New York, NY: John Wiley & Sons, 1998.